Nanomesh-patterning on multilayer MoS2 field-effect transistors for ultra-sensitive detection of cortisol

Heekyeong Park
Kyung Hee University
Seungho Baek
Sungkyunkwan University
Bongjin Jeong
Electronics and Telecommunications Research Institute (ETRI) https://orcid.org/0000-0001-6536-7215
Anamika sen
Sungkyunkwan University
Sehwan Kim
Sungkyunkwan University
Yun Chang Park
National Nanofab Center
Sunkook Kim (seonkuk@khu.ac.kr)
Sungkyunkwan University https://orcid.org/0000-0003-3724-6728
young jun kim
Electronics and Telecommunications Research Institute (ETRI)

Article

Keywords: nanomesh-patterning, cortisol, molybdenum disulfide

Posted Date: September 2nd, 2020

DOI: https://doi.org/10.21203/rs.3.rs-64919/v1

Abstract

Absence of functional groups on the basal plane of molybdenum disulfide (MoS_2) significantly hinders the performance of MoS_2 field-effect transistor-based biosensor (bio-FET). We present a novel method for creating nano-scale holes on a MoS_2 channel using block copolymer lithography, where the edge areas on the nanoholes were used to form covalent linkage between the capture molecules of cortisol aptamer and the MoS_2 channel. The comparative analysis of Raman and XPS spectra well supported the formation of the nanoholes on MoS_2 together with the concomitant increase in the edge area. The performance of the nanomesh bio-FET was studied by comparing its detection behavior for cortisol with that of a bio-FET manufactured with pristine MoS_2. The nanomesh MoS_2 bio-FET detected cortisol 10^9 times as low as that by the pristine MoS_2 bio-FET. The selectivity of the nanomesh bio-FET was validated by detection experiments with other steroid hormones and antigens. Additionally, clinical applicability was demonstrated by performing experiments in artificial saliva and human serum.

Introduction

Field-effect transistors (FETs), with intrinsic advantages that allow label-free, rapid, and ultra-sensitive detection of target molecules[1–3], are highly desired as biosensors for a wide range of medical care[4], agricultural[5], and environmental[6] applications. Under suitable conditions, FET-based biosensors (bio-FETs) are capable of more sensitive conversion of the specific interaction between target molecules and receptor elements. More importantly, the detection performance of bio-FETs largely depends on the structural and electrical characteristics of the channel materials, thereby opening opportunities to further enhance assay performance by devising specific nanostructures. One-dimensional (1D) nanomaterials, including silicon nanowires and carbon nanotubes, have been investigated to improve sensing performance; however, their complex manufacturing and integration processes are major hindrances to their commercialization[7]. Among two-dimensional (2D) nanomaterials, transition metal dichalcogenides (TMDs) are considered promising materials for ultra-sensitive biosensors because of their intrinsic carrier transport and modulation in contrast to graphene, which has zero band gap[8–10].

However, in spite of the intrinsic properties of their 2D structure, the use of TMD materials for applications in biosensors has not been very successful mainly due to the limited number of functional groups on the TMD surface. Conventional bio-FETs based on TMDs contain a dielectric layer such as hafnium oxide (HfO_2) or aluminum oxide (Al_2O_3), as a grafting layer to functionalize the bioreceptors on the top of TMD channels[8, 11, 12]. The surface of the oxide layer enables the chemical functionalization of bioreceptors using 3-aminoproplytriethoysilane (APTES) and glutaraldehyde. However, the dielectric effect on the screening of biomolecular charges deteriorates the sensitivity of bio-FETs[13, 14]. In addition, interface defects between the channel and dielectric layer can create incidental electric fields or parasitic coupling, further reducing the sensitivity and reliability of bio-FETs[15]. In an effort to circumvent the problem related to functionalization, surface defect engineering is applied to generate dangling bonds on the TMD

surface. Sim et al.[16] reported the artificial formation of sulfur vacancies on molybdenum disulfide (MoS_2) for the direct attachment of functional molecules on the MoS_2 surface. In addition, Lee et al.[17] reported defect generation on a tungsten diselenide (WSe_2) surface using oxygen (O_2) plasma treatment to functionalize the bioreceptors on the surface.

In this work, we applied a nanomesh structure on MoS_2 via block copolymer (BCP) lithography, where newly generated dangling groups on the edges of the perforated area would provide a rich source for functionalization. Moreover, direct covalent linkage between MoS_2 and the biorecognition element could avoid sensitivity and reliability losses. Indeed, periodically arranged nanoholes on the MoS_2 nanomesh consisting of abundant edge sites were confirmed by scanning transmission electron microscopy (STEM), Raman, and X-ray photoelectron spectroscopy (XPS) spectroscopic analysis. These edge defects allow direct functionalization of the receptors on the MoS_2 nanomesh channel for ultra-sensitive detection of biomolecules. Cortisol, a target biomolecule, is a glucocorticoid steroid hormone secreted through the hypothalamus-pituitary-adrenal (HPA) axis. Repeated activation of the HPA axis has been reported to negatively affect mental health, causing major depressive disorder[18], anxiety disorder[19], and bipolar disorder[20]. Aptamer-functionalized MoS_2 nanomesh FETs exhibit excellent detection properties for cortisol biomarkers with a low limit of detection (LOD) of 10^{-18} g/mL, in environments including artificial saliva and real human serum. Furthermore, high selectivity for other molecules and steroid hormones was also confirmed, thus, verifying the high reliability of the proposed nanomesh architecture for high-performance biosensors.

Results

Nano-scale patterning of multilayer MoS_2

Various nanomaterials have been used for high-performance biosensors by designing sophisticated schemes but often with complicated procedures. Multilayered MoS_2, an extension of 2D materials, although endowed with intrinsic morphological advantages as a sensor, is unsuitable for applications as biosensor due to the absence of functional groups upon which the capture molecules can be attached. In this study, the functionality problem was overcome by generating innumerable nano-sized holes of uniform diameter on MoS_2. We established a procedure for the fabrication of the MoS_2 nanomesh structure using the BCP self-assembly layer as a nanomesh template (Fig. 1a). Multilayered MoS_2 nanosheets, physically exfoliated from its bulk, were passivated by depositing a 10 nm thick silicon oxide (SiO_2) layer, which plays an important role in preventing chemical damage on the MoS_2 surface during the patterning process. The spin-coated BCP layer underwent a cylindrical microphase separation between domains of polystyrene (PS) and polymethyl methacrylate (PMMA) at an elevated temperature of 230 °C. The minor phase of the PMMA domain was selectively removed through ultraviolet (UV) exposure, leaving the PS phase intact in mesh morphology. The nanomesh fabrication procedure was completed by washing with acetic acid. A scanning electron microscopy (SEM) image of the BCP

template is shown in Supplementary Fig. 1a, indicating the characteristic ordering of nanoporous structures over a large area with a uniform hole diameter (20.7 ± 1.3 nm). The nanomesh template was treated with O_2 plasma reactive-ion etching (RIE) to control the hole size of the BCP template. The nanomesh structure of MoS_2 was constructed using the BCP template as a patterning mask, in which the SiO_2 layer was etched away by sulfur hexafluoride (SF_6) plasma RIE and the MoS_2 was perforated by boron trichloride (BCl_3) plasma RIE. The remaining SiO_2 was easily removed by dipping the substrate into buffered oxide etchant (BOE), leaving no trace of contaminants. The detailed process is described in the Methods section. The SEM images of the MoS_2 surface for each process are shown in Supplementary Fig. 1.

Figure 1b shows a low-magnification STEM image of the multilayered MoS_2 nanomesh film, revealing periodically organized nanoholes in hexagonally packed ordering. The structural uniformity of the nanoholes was confirmed by measuring the diameter of 2,200 nanoholes, which was calculated to be 23.36 nm with a standard deviation of 1.5 nm (Fig. 1c). Further, the vertically oriented nanohole structure across the multilayered MoS_2 was confirmed by a cross-sectional STEM image, as shown in Fig. 1d, where the nanohole areas look brighter than the unperforated areas owing to differences in the distance from the MoS_2 atoms to the objective lens of the STEM. In the brighter nanohole area, 10 MoS_2 layers can be clearly observed.

Spectroscopic analysis of MoS_2 nanomesh

Figure 2a shows a highly magnified STEM image of the multilayered MoS_2 nanomesh with a close-up view of the dashed area presented in Fig. 2b, which well supports a nanohole perforated on (100)-oriented hexagonal 2H MoS_2 film. Indeed, the intensity mapping images (Fig. 2c and d) exhibit anisotropically etched edge configurations of the perforated MoS_2 multilayer, representing a clear increase in the randomly distributed edge area in both the horizontal and vertical directions.

To study the effects of the newly formed morphological changes in MoS_2, a comparative analysis was performed for both the nanomesh and pristine MoS_2 films using Raman and XPS. In the Raman spectra (Fig. 2e), 2 characteristic Raman peaks of the in-plane, E^1_{2g}, and out-of-plane, A_{1g}, vibrations were observed at 380 and 407 cm^{-1}, respectively, in both the pristine and the nanomesh MoS_2[21]. After perforation, the relative intensities of the in-plane and out-of-plane vibrations (E^1_{2g}/A_{1g}) decreased from 0.802 for the pristine to 0.613 for the nanomesh MoS_2. The lowering of E^1_{2g}/A_{1g} in the nanomesh MoS_2 supports the presence of the newly generated nanoholes and increase in the edge sites, because A_{1g} vibration is preferentially excited to the E^1_{2g} vibration for edge-terminated films[22, 23].

Figure 2f shows XPS analysis of the nanomesh and pristine MoS_2 films with regard to their Mo 3*d* core levels. The corresponding S 2*p* spectra are shown in Supplementary Fig. 2a. In the Mo 3*d* spectra, the

peak is deconvoluted into three different types of Mo ligands corresponding to the intrinsic MoS_2 (i-MoS_2), defective MoS_2 (d-MoS_2), and molybdenum oxide (MoO_x)[24, 25]. In the doublet of i-MoS_2, the maximum peak at around 229.10 eV (Mo^{4+} $3d_{5/2}$), which corresponds to 2H stoichiometric MoS_2 (ratio of S/Mo = 2), was observed in both the pristine and nanomesh MoS_2 films with high intensity. The maximum peak of the d-MoS_2 at ~ 228.50 eV (Mo^{4+} $3d_{5/2}$) is relatively small, corresponding to the nonstoichiometric MoS_2 (S/Mo ratio < 2) introduced by atomic defects on the film, such as vacancies and exposed edges[24]. These defect sites have electronic structures different from those of the intrinsic MoS_2 owing to the unstable energy state, resulting in peak excitation at lower binding energies. The atomic fraction of d-MoS_2 among the total Mo ligands was calculated to be 6.18% for the pristine MoS_2 film, which significantly increased to 15.82% for the MoS_2 nanomesh film (Table 1). This can be seen as evidence of the quantitative increase in the active edge sites in the MoS_2 nanomesh. In addition, the increase in nonstoichiometric MoS_2 causes the characteristic broadening of the S 2*p* doublet, with a concomitant increase in the full width at half maximum (FWHM) from 0.68 to 0.89 (Supplementary Fig. 2a and Table 1). Contaminations on the active edge sites may occur during the etching process with BCl_3 plasma RIE. However, the absence of a Cl 2*p* peak in the MoS_2 nanomesh film (Supplementary Fig. 2b) indicates that no contamination occurred during the BCl_3 etching process. In addition, the atomic fraction of Mo^{6+} 3*d* (MoO_x) at approximately 232.53 eV barely changed from 11.93% for the pristine to 11.49% for the nanomesh MoS_2, indicating that the active edge regions were not oxidized on exposure to atmosphere.

Table 1

at% (FWHW)	i-MoS_2 ($Mo^{4+}3d_{5/2}$) [229.10±0.2 eV]	d-MoS_2 ($Mo^{4+}3d_{5/2}$) [228.50±0.2 eV]	MoO_x (Mo^{6+} $3d_{5/2}$) [232.53 eV]	S_2Mo ($S^{2-}2p_{3/2}$) [161.95 eV]
Pristine MoS_2	81.88% (0.71)	6.18% (1.01)	11.93% (1.72)	100% (0.68)
MoS_2 nanomesh	72.70% (0.88)	15.82% (1.00)	11.49% (1.56)	100% (0.89)

Operation of the MoS_2 nanomesh FET

To explore the electrical characteristics of the multilayer MoS_2 nanomesh, we fabricated FETs using MoS_2 nanomesh films as channels (Fig. 3a). The SEM image of the MoS_2 nanomesh FET shows uniform nanoholes across the channel area positioned between the two titanium/gold (Ti/Au) electrodes (Fig. 3b). Figure 3c depicts the transfer characteristics of the MoS_2 nanomesh FET in logarithmic (black) and linear

(red) scales measured under a gate voltage (V_{GS}) from − 40 to 40 V at a drain voltage (V_{DS}) of 1 V. The length (L) and width (W) of the nanomesh channel were 7 μm and 16.56 μm, respectively. It demonstrated an n-type semiconductor behavior with an on–off ratio (I_{on}/I_{off}) of 7.28. × 10^4 and a field-effect mobility (μ) of 6.56 $cm^2\ V^{-1}\ s^{-1}$. Compared to the high μ and I_{on}/I_{off} values of typical multilayer MoS_2 FETs reported in literature[26], the relatively low values of the MoS_2 nanomesh FET are thought to have been caused by an increase in carrier trapping and scattering in the MoS_2 channel introduced by the increase in defective edge areas[27]. The statistical distribution of the electrical performances for 20 different MoS_2 nanomesh FETs is described in Supplementary Table 1. Figure 3d shows the output characteristics of the FET measured in V_{GS} from − 40 to 0 V with intervals of 10 V, showing excellent n-type property and drain current (I_{DS}) saturation at a high V_{DS} region.

Sensing performance of the MoS_2 nanomesh bio-FET for cortisol

Although the increase in edge sites upon generating nanoholes produced a detrimental effect on the electrical performance, when the nano-patterned MoS_2 FET was applied to biosensors, the edge sites turned out to clearly enhance the detection performance. Figure 4a describes the general procedure for preparing the MoS_2 nanomesh bio-FET, in which MoS_2 nanomesh FET treated with O_2 plasma was functionalized with cortisol aptamer using the well-known APTES-glutaraldehyde chemistry followed by blocking with casein[28]. The O_2 plasma was applied at mild conditions (5 sccm, 10 W, 15 s) to minimize any possible damage to the nanomesh structure as it may have a detrimental effect on its electrical properties. To understand the chemical nature of the plasma-treated MoS_2 nanomesh, XPS analysis was carried out for the nano-patterned MoS_2 (Supplementary Fig. 3). While the oxidation process produced MoO_x on the edge, unstable oxide layer $MoS_{2-x}O_x$ was formed on the basal plane (The details were discussed in the Supporting information).

The sensing behavior of the MoS_2 nanomesh bio-FET was studied by gradually adding cortisol stepwise so that the target concentration could be adjusted as required. Highly sensitive variation of I_{DS}– V_{GS} curves was observed upon exposure to cortisol, as shown in Fig. 4b. To better understand the effect of nanohole formation in MoS_2 on the sensing behavior, the sensing characteristics of the nanomesh and pristine MoS_2 FETs were compared by repeating the experiment using multiple devices. The sensing behavior of pristine MoS_2 is shown in Supplementary Fig. 4 with an enlarged view of the vertical scale. The sensitivity was calculated based on $(I_{base} - I_{cortisol})/I_{base}$ x 100, where I_{base} and $I_{cortisol}$ are the values before and after the addition of cortisol, respectively, at V_{GS} of 10 V. While a typical S-shaped response pattern with a wide linear range from 10^{-18} g/mL to 10^{-13} g/mL was observed for the nanomesh MoS_2 FET, in the case of pristine FET, no apparent variation in the response signal was observed except over 10^{-9} g/mL. Surprisingly, the generation of nanoholes in MoS_2 contributed to an increase in sensing

performance 10^9 times that of pristine MoS_2. Such a superb enhancement in sensing behavior is thought to have been caused by the increased edge area provided by the newly generated nanoholes in MoS_2, which in turn enabled direct chemical bonding between the aptamers and MoS_2 with concomitant augmentation of polarity modulation.

Sensor reliability

The reliability of the nanomesh bio-FET was examined by studying the extent of nonspecific binding and selectivity using potentially interfering biomolecules. To understand the level of nonspecific interaction that might have been generated due to nanohole formation in MoS_2, cortisol detection was performed using nanomesh FETs in the absence of the aptamer capture molecules, specifically the nanomesh FET in which the surface chemistry was altered only up to the functionalization step of glutaraldehyde. No appreciable signal change was detected (Fig. 4d), suggesting that nonspecific interaction was negligible.

In addition, the selectivity of the MoS_2 nanomesh biosensor for target cortisol was evaluated by measuring the electrical signals on exposure to potentially interfering biomolecules, including steroid hormones of progesterone and aldosterone, and protein biomarkers of alpha-fetoprotein (AFP), prostate specific antigen (PSA), and carcinoembryonic antigen (CEA) (Fig. 4e). The differences in the signal intensity before and after exposure ($|\Delta I_{DS}|$) to the protein antigens were below recognizable levels, whereas in the case of the steroid hormones, only slight differences in signal intensities were observed. It is worthwhile to note that the chemical structure of cortisol is very similar to that of progesterone and aldosterone.

Saliva and serum test

One major advantage of using cortisol as a biomarker is the diverse availability of its biological fluids, including serum, urine, sweat, and saliva. In particular, measuring cortisol concentration in saliva has multiple merits, including being a patient-friendly noninvasive detection method and direct measurement of free unbound cortisol, which is a biologically active form; 90% of cortisol circulates in complexation with globulin[29]. To study the applicability of the nanomesh MoS_2 bio-FET in the clinical environment, the detection behavior of the bio-FET was examined in the media of artificial saliva and human serum. Figure 5a shows I_{DS}– V_{GS} curves when the detection test was performed by varying the amount of cortisol from 10^{-18} g/mL to 10^{-8} g/mL in artificial saliva including the control test. Well separated signals are evident especially at low concentration range with gradual decrease in distance between signals at higher concentration window. This tendency was somewhat more pronounced in the case of artificial saliva than human serum (Fig. 5b). The I_{DS}– V_{GS} curves for real humans are shown in Supplementary Fig. 5. When compared with the results from the buffer test, the detection performance in the artificial saliva and serum seemed to have decreased to some extent, especially in the low concentration range. However, the LOD remained at 10^{-18} g/mL with linearity ranging up to 10^{-12} g/mL in those biological fluids.

Conclusion

Superb enhancement in sensing performance was achieved by providing nanohole structures in MoS_2. BCP nanotemplates produced periodically organized nanoholes on the MoS_2 surface, thus introducing abundant edge sites. The generation of edge sites on the MoS_2 surface resulted in degradation of the electrical performance for FET while offering extremely high sensitivity for bio-FET by inducing direct functionalization of the edge sites using cortisol aptamer. We confirmed the ultra-high sensitivity by comparing it with the sensing properties of bio-FETs based on pristine MoS_2. In addition, the nanomesh bio-FET functionalized with aptamer exhibited reasonable selectivity for cortisol compared to other steroids and antigens, including progesterone, aldosterone, AFP, PSA, and CES. Clinical applicability was also confirmed by performing the test on artificial saliva and real human serum. The excellent detection performance of the MoS_2 nanomesh bio-FET was confirmed by realizing an ultra-low LOD of 10^{-18} g/mL, which verified the potential of our effective platform for future biosensor applications and new diagnostic processes.

Materials And Methods

Fabrication of the MoS_2 nanomesh FET. The general fabrication process of the MoS_2 nanomesh consists of organizing the BCP nanopattern on MoS_2, etching the MoS_2, and subsequently removing the upper BCP layers. Multilayered MoS_2 nanosheets were placed on a Si/SiO_2 substrate by mechanical exfoliation from bulk MoS_2. A 10 nm thick SiO_2 layer was deposited onto the MoS_2 nanosheets using an electron-beam (e-beam) evaporator. A 1 wt% solution of poly (styrene-*r*-methyl methacrylate) (PS-*r*-PMMA) (M_n = 8,500 M_w/M_n = 1.45, styrene content 66%, α-hydroxyl-ω-TEMPO moiety terminated) random copolymer (RCP) in toluene was spin-coated on the MoS_2 films at 3,000 rpm, followed by substrate annealing at 250 °C for 2 h under vacuum and finally rinsing with toluene. A solution of 1 wt% poly(styrene-*b*-methyl methacrylate) (PS-*b*-PMMA) (PS:PMMA = 55,000 : 22,000, M_w/M_n = 1.09) BCP in toluene was also spin-coated with the same protocol as RCP and annealed at 230 °C. The PMMA portions in the BCP thin film were decomposed by UV irradiation (wavelength of 254 nm) for 30 min and finally dissolved in acetic acid solution. O_2 plasma RIE (10 sccm, 10 W, 10 s) was applied to the surface of BCP. SF_6 plasma RIE (10 sccm, 200 W, 15 s) was carried out to punch nanoholes on the SiO_2 layer. Subsequently, BCl_3 plasma RIE (10 sccm, 100 W) was used to make MoS_2 nanoholes, with the plasma treatment time varying with the thickness of MoS_2. At the end of the process, the substrate was submerged in BOE for 1 s to eliminate the remaining SiO_2 and BCP on the MoS_2 nanomesh. To construct the FET on the prepared MoS_2 nanomesh, the source and drain were prepatterned by photolithography and a lift-off process, followed by deposition of Ti (20 nm)/Au (100 nm) by e-beam evaporation.

Characterizations. Microstructural studies of the MoS_2 nanomesh were conducted using STEM (HD-2300A, Hitachi) with an accelerating voltage of 200 kV. For plane-view observation, the MoS_2 nanomesh films were transferred onto Cu grids coated with a lacey carbon film. A cross-sectional view was observed

by milling the sample using a single-beam focused ion-beam (FB-2100, Hitachi). Low-magnification surface images were obtained by SEM operated at an acceleration voltage of 15 kV and working distance of 8 mm. Raman spectroscopy (ALPHA300, WITec) was used to identify the formation of edge sites on MoS_2 nanosheets. A laser beam with a spot diameter of 1 μm and excitation wavelength of 532 nm was used, and the instrument spectral resolution was approximately 1 cm^{-1}. The chemical states of the MoS_2 films were explored by XPS (K-Alpha, Thermo Fisher Scientific) using an Al *K*α source. All electrical measurements were carried out using a semiconductor characterization analyzer (4200-SCS, Keithley) equipped with a probe station for sample loading and electrode contact.

MoS_2 surface modification and biosensing processes. Specific detection of cortisol was facilitated by functionalizing an aptamer, which is a bioreceptor for cortisol, on the channel surface of the MoS_2 nanomesh bio-FET. The aptamer (Bioneer) was dissolved in Tris-HCl (pH 8.0) solution to obtain a concentration of 10^{-6} g/mL. The MoS_2 bio-FET was first exposed to O_2 plasma (10 sccm, 10 W, 15 s) for edge oxidation. The MoS_2 was then functionalized with APTES by treating with a solution of APTES in a 19:1 (v/v) mixture of ethanol and deionized (DI) water for 3 h. Subsequently, the device was rinsed in ethanol and dried at 120 °C for 15 min. To convert the amine functional group of APTES to an aldehyde group, the device was immersed in 4.5 mL of glutaraldehyde solution consisting of 0.1 g of $NaCNBH_4$, 1 tablet of phosphate buffered saline (PBS), and 200 mL of DI water, for 2 h, followed by rinsing in DI water. The device was incubated overnight in a 10^{-6} g/mL aptamer solution in Tris-HCl (pH 8.0) at 4 °C. To prevent nonspecific binding, 1% (w/v) casein blocker (Thermo Fisher Scientific) was added to the device for 1 h at room temperature. For the detection of cortisol, 16 different concentrations of cortisol solution (Sigma Aldrich) ranging from 10^{-21} g/mL to 10^{-6} g/mL were dissolved in PBS solution (pH 7.4). Each cortisol solution was dropped onto the device for 30 min and subsequently rinsed and dried for electrical measurements.

Detection in saliva and human serum. To understand the sensing behavior in the biological environment of saliva and serum, different concentrations of cortisol were dissolved in artificial saliva and real human serum. Real human serum was purchased from Sigma Aldrich. Artificial saliva was prepared by dissolving 5 mM NaCl, 1 mM $CaCl_2$, 15 mM KCl, 1 mM citric acid, 1.1 mM KSCN, and 4 mM NH_4Cl in distilled water.

Declarations

Competing interest

The authors declare no competing financial interests.

Author contributions

S. Kim and Y. J. Kim designed this experiment and application. H. Park and A. Sen fabricated the MoS_2 nanomesh using BCP lithography and conducted characterizations of the materials. S. Baek, B. Jung, and S. Kim measured the sensing properties of MoS_2 nanomesh bio-FETs. Y. C. Park contributed to the structural analysis of MoS_2 nanomesh using STEM combined with EDX. All authors wrote and contributed to the manuscript.

Acknowledgements

This research was supported in part by the National Research Foundation of Korea (2018R1A2B2003558). This research was supported by the Bio & Medical Technology Development Program of the National Resarch Foundation (NRF) through funding from the Ministery of Science & ICT (NRF-2014M3A9D7070779).

References

1. Vigneshvar, S., Sudhakumari, C. C., Senthilkumaran, B. & Prakash, H. Recent advances in biosensor technology for potential applications - an overview. *Front. Bioeng. Biotech.* 4, 11 (2016).
2. Perumal, V. & Hashim, U. Advances in biosensors: principle, architecture and applications. *J. Appl. Biomed.* 12, 1–15 (2014).
3. Sarkar, D. & Banerjee, K. Proposal for tunnel-field-effect-transistor as ultra-sensitive and label-free biosensors. *Appl. Phys. Lett.* 100, 143108 (2012).
4. Poghossian, A. et al. Possibilities and limitations of label-free detection of DNA hybridization with field-effect-based devices. *Sens. Actuators B Chem.* 111, 470–480 (2005).
5. Rai, V., Acharya, S. & Dey, N. Implications of nanobiosensors in agriculture. *J. Biomater. Nanobiotech.* 03, 02 (2012).
6. Rodriguez-Mozaz, S., de Alda, M. J. L., Marco, M. P. & Barcelo, D. Biosensors for environmental monitoring - a global perspective. *Talanta* 65, 291–297 (2005).
7. Makowski, M. S. & Ivanisevic, A. molecular analysis of blood with micro-/nanoscale field-effect-transistor biosensors. *Small* 7, 1863–1875 (2011).
8. Sarkar, D. et al. MoS_2 field-effect transistor for next-generation label-free biosensors. *ACS Nano* 8, 3992–4003 (2014).
9. Kalantar-zadeh, K. et al. Two-dimensional transition metal dichalcogenides in biosystems. *Adv. Func.Mater.* 25, 5086–5099 (2015).
10. Park, H. et al. MoS_2 field-effect transistor-Amyloid-beta$_{(1-42)}$ hybrid device for signal amplified detection of MMP-9. *Anal. Chem.* 91, 8252–8258 (2019).
11. Nam, H. et al. Multiple MoS_2 transistors for sensing molecule interaction kinetics. *Sci. Rep.* 5, 10546 (2015).

12. Wang, L. et al. Functionalized MoS_2 nanosheet-based field-effect biosensor for label-free sensitive detection of cancer marker proteins in solution. *Small* 10, 1101–1105 (2014).
13. Ahn, J. H. et al. Charge and dielectric effects of biomolecules on electrical characteristics of nanowire FET biosensors. *Appl. Phys. Lett.* 111, 113701 (2017).
14. Liu, Y. & Dutton, R. W. Effects of charge screening and surface properties on signal transduction in field effect nanowire biosensors. *J. Appl. Phys.* 106, 014701 (2009).
15. Kovacevic, G. & Pivac, B. Structure, defects, and strain in silicon-silicon oxide interfaces. *J. Appl. Phys.* 115, 043531 (2014).
16. Sim, D. M. et al. Controlled doping of vacancy-containing few-layer MoS_2 via highly stable thiol-based molecular chemisorption. *ACS Nano* 9, 12115–12123 (2015).
17. Lee, H. W. et al. Highly sensitive and reusable membraneless field-effect transistor (FET)-type tungsten diselenide (WSe_2) biosensors. *ACS Appl. Mater. Interfaces* 10, 17639–17645 (2018).
18. Kendler, K. S., Karkowski, L. M. & Prescott, C. A. Causal relationship between stressful life events and the onset of major depression. *Am. J. Psychiatry* 156, 837–841 (1999).
19. Moreno-Peral, P. et al. Risk factors for the onset of panic and generalised anxiety disorders in the general adult population: a systematic review of cohort studies. *J. Affect. Disord.* 168, 337–348 (2014).
20. Agnew-Blais, J. & Danese, A. Childhood maltreatment and unfavourable clinical outcomes in bipolar disorder: a systematic review and meta-analysis. *Lancet Psychiat.* 3, 342–349 (2016).
21. Li, H. et al. From bulk to monolayer MoS_2: evolution of raman scattering. *Adv. Func. Mater.* 22, 1385–1390 (2012).
22. Yun, T. et al. 2D metal chalcogenide nanopatterns by block copolymer lithography. *Adv. Func. Mater.* 28, 1804508 (2018).
23. Kim, T. et al. Structural defects in a nanomesh of bulk MoS_2 using an anodic aluminum oxide template for photoluminescence efficiency enhancement. *Sci. Rep.* 8, 6648 (2018).
24. Kondekar, N. P., Boebinger, M. G., Woods, E. V. & McDowell, M. T. In situ XPS investigation of transformations at crystallographically oriented MoS_2 interfaces. *ACS Appl. Mater. Interfaces* 9, 32394–32404 (2017).
25. Lin, H. B. et al. Electrocatalysis of polysulfide conversion by sulfur-deficient MoS_2 nanoflakes for lithium-sulfur batteries. *Energy Environ. Sci.* 10, 1476–1486 (2017).
26. Kim, S. et al. High-mobility and low-power thin-film transistors based on multilayer MoS_2 crystals. *Nat. Commun.* 3, 1011 (2012).
27. Chen, S. H. et al. Monolayer MoS_2 nanoribbon transistors fabricated by scanning probe lithography. *Nano Lett.* 19, 2092–2098 (2019).
28. Park, H. et al. Label-free and recalibrated multilayer MoS_2 biosensor for point-of-care diagnostics. *ACS Appl. Mater. Interfaces* 9, 43490–43497 (2017).

29. Estrada-Y-Martin, R. M. & Orlander, P. R. Salivary cortisol can replace free serum cortisol measurements in patients with septic shock. *Chest* 140, 1216–1222 (2011).

Figures

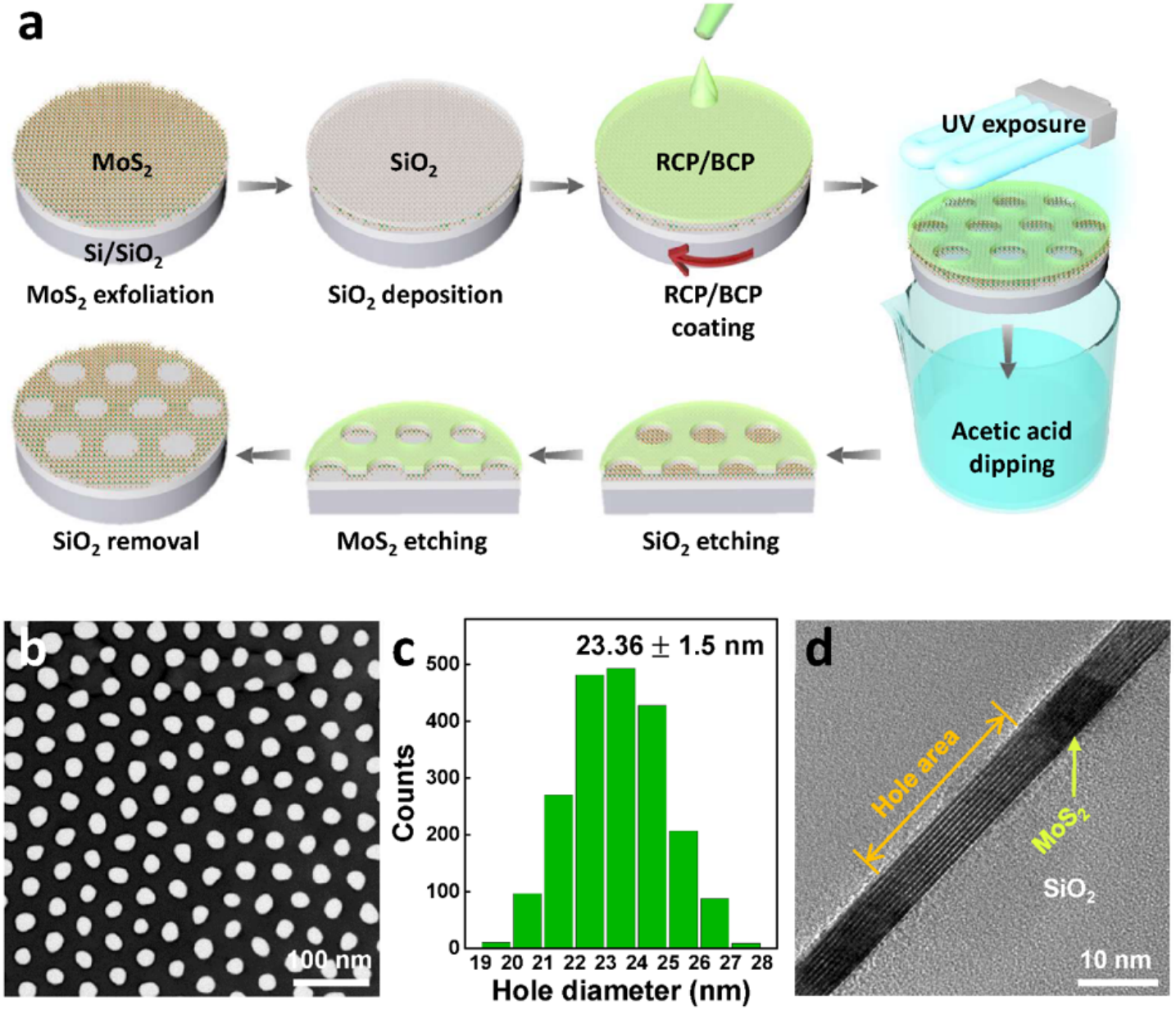

Figure 1

Fabrication process and microscopic characterization of multilayer MoS2 nanomesh. a, Schematic illustrations of fabrication procedure of multilayer MoS2 nanomesh. b, Low-magnification STEM image of multilayer MoS2 nanomesh film. c, Statistical distribution of the hole diameters on MoS2 nanomesh. d, Cross-sectional STEM image of the multilayer MoS2 nanomesh.

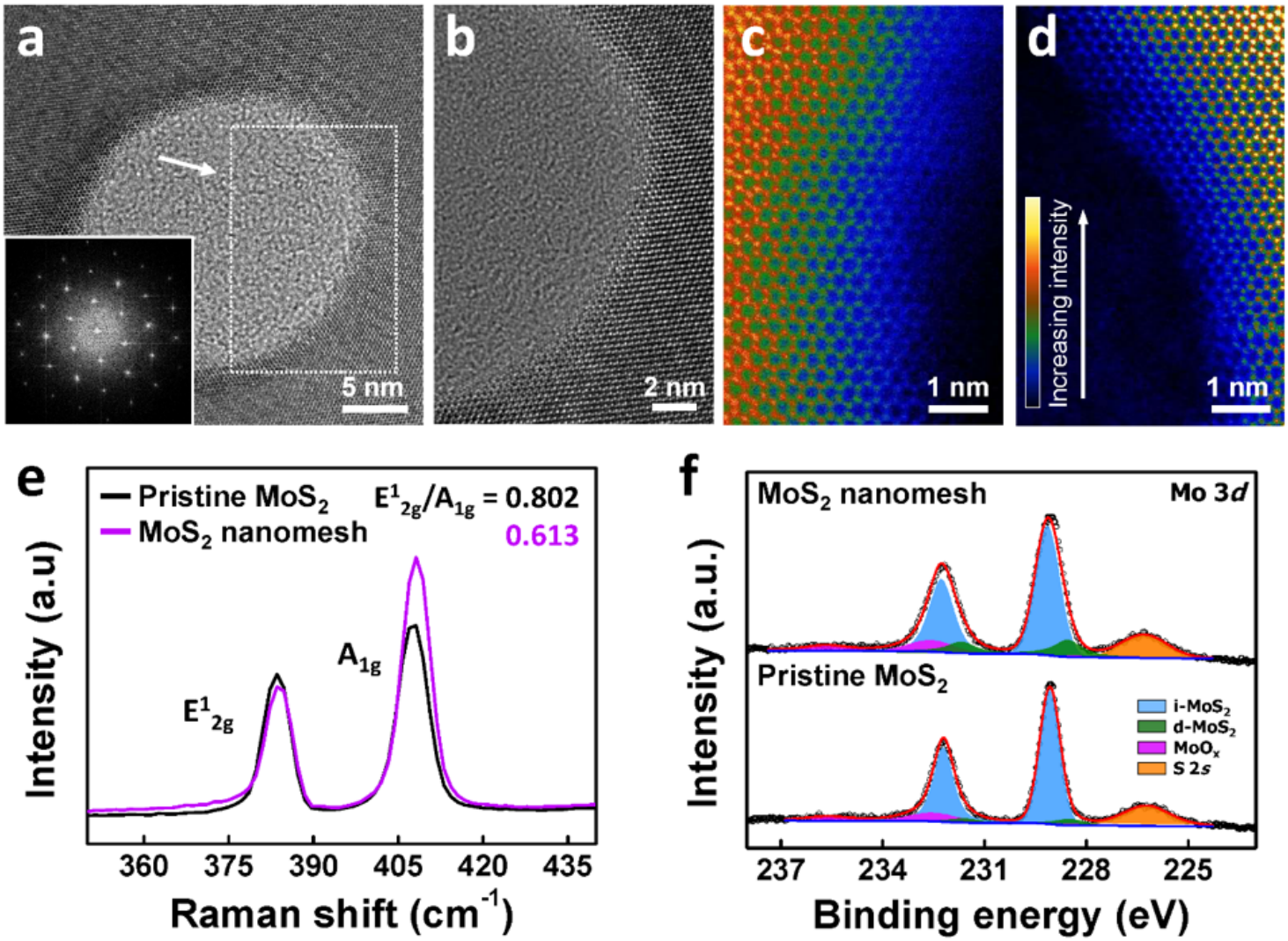

Figure 2

Structure and spectroscopic characterization of multilayer MoS2 nanomesh. a, Plan-view STEM image of nanoholes with FFT pattern corresponding to (100)-oriented hexagonal 2H MoS2 plane. b, high-magnification STEM image of the marked area in a. c and d, Intensity mapping images of the edge area of MoS2 nanohole. e, Raman and f, XPS spectra of multilayer MoS2 before and after nanomesh patterning.

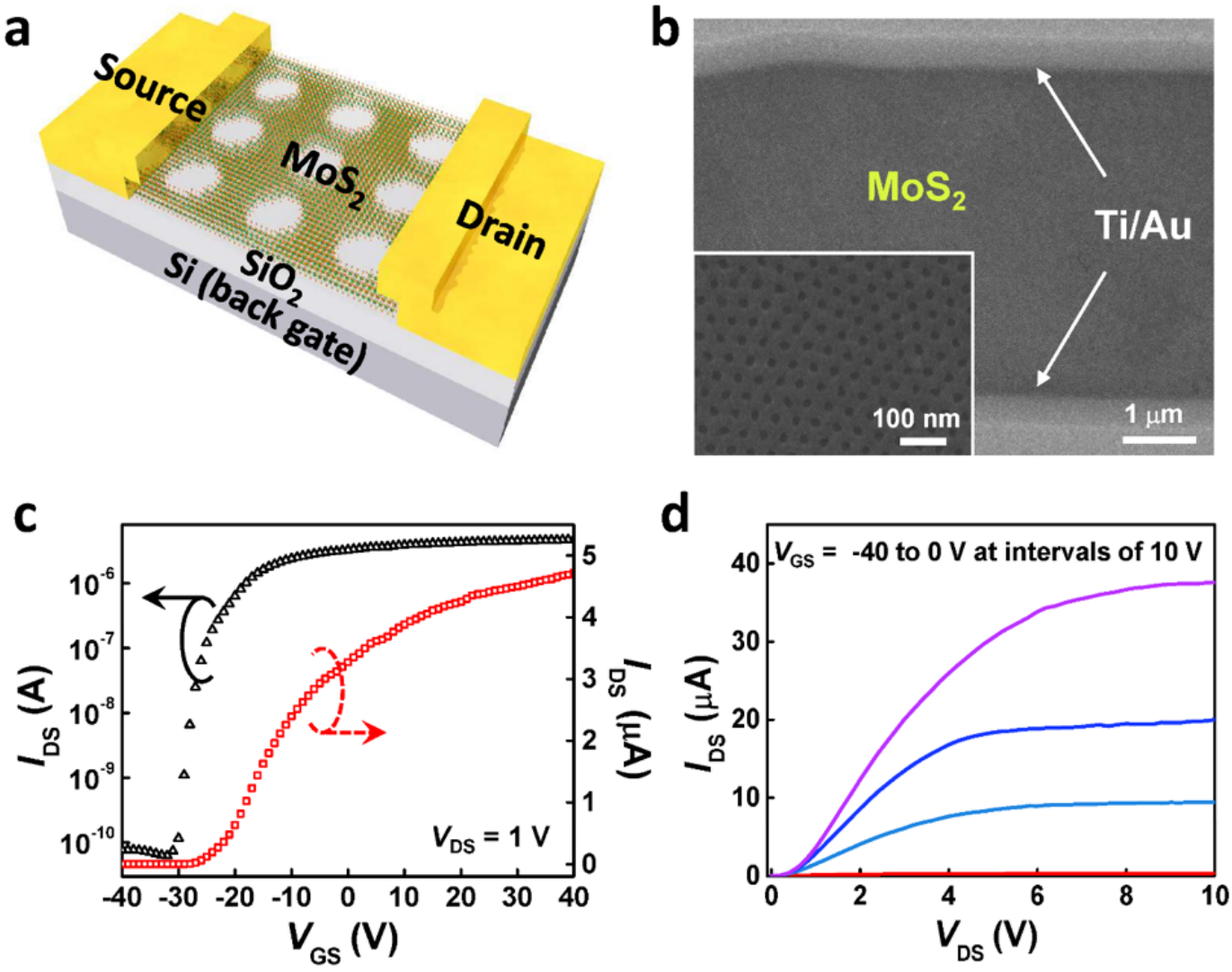

Figure 3

Electrical properties of MoS2 nanomesh FET. a, A schematic and b, SEM images of MoS2 nanomesh FET. c, Transfer and d, output characteristics of MoS2 nanomesh FET.

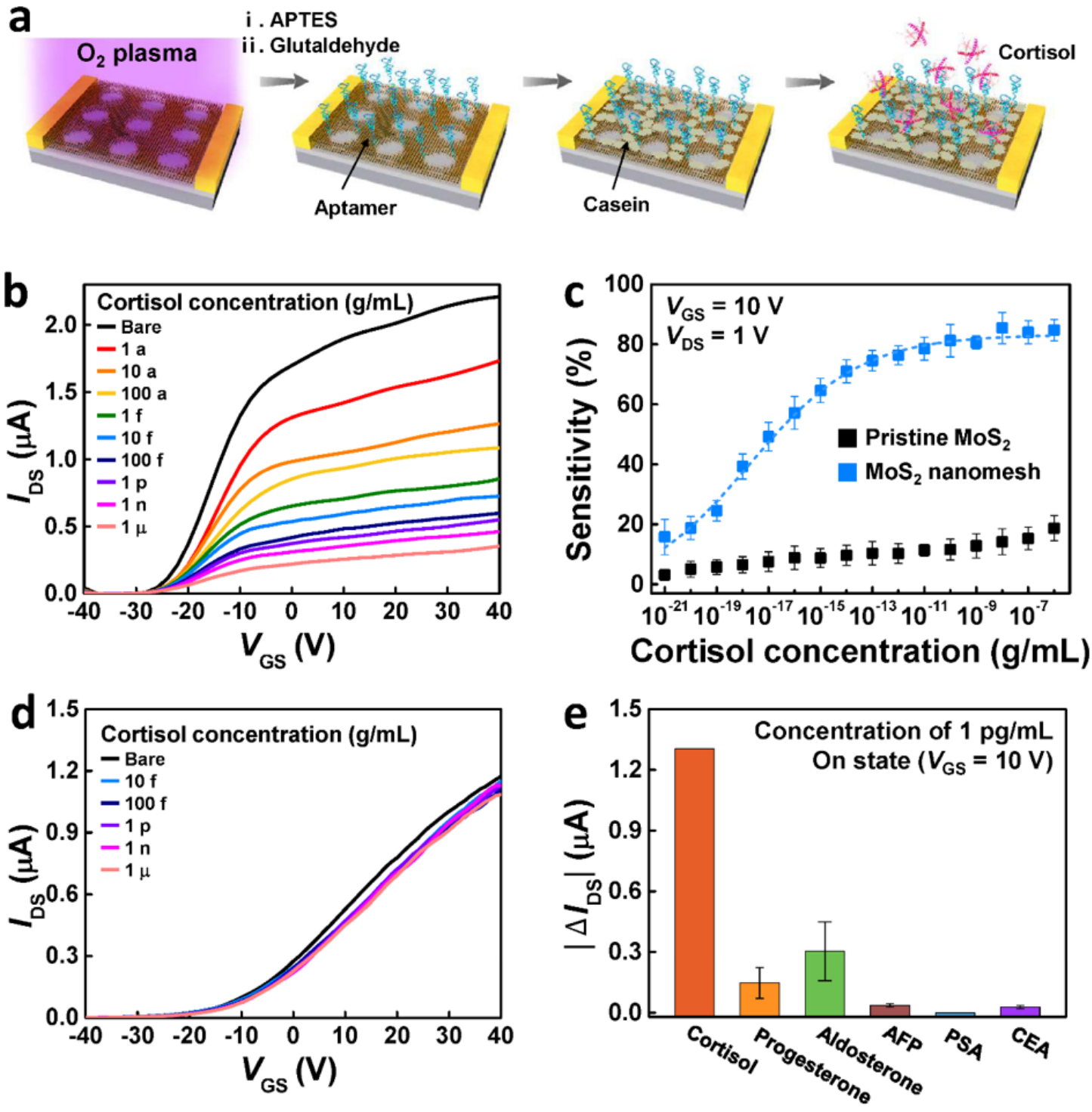

Figure 4

Detection characteristics of multilayer MoS2 nanomesh bio-FETs. a, Experimental process of functionalization of aptamer on surface of MoS2 nanomesh and the detection of cortisol. b, Transfer characteristics of aptamer-immobilized MoS2 nanomesh bio-FET with increasing cortisol concentrations. c, A comparison of sensitivity of nanomesh and pristine MoS2 bio-FETs according to contisol concentrations. d, Transfer behavior of MoS2 nanomesh bio-FET unimmobilized with aptamer for

different concentrations of cortisol. e, Selectivity test of MoS2 nanomesh bio-FETs for cortisol detection with several potentially interfering steroid hormones and antigens.

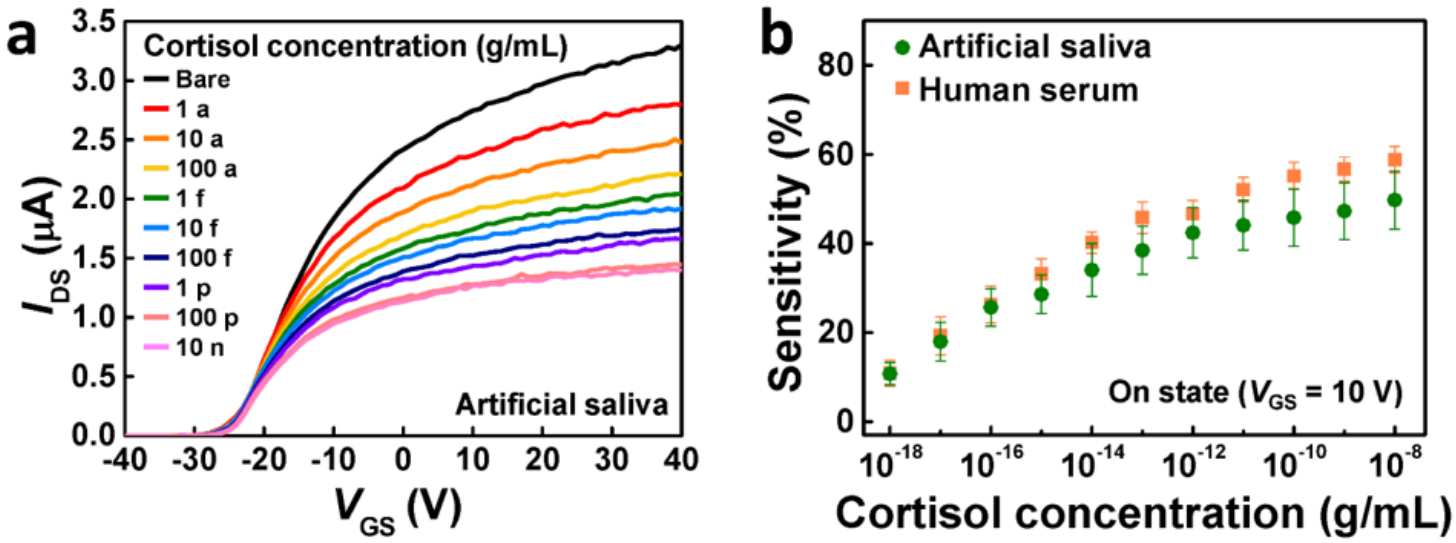

Figure 5

Detection behavior of MoS2 nanomesh bio-FETs in saliva and serum a, Detection characteristics of MoS2 nanomesh bio-FET for different concentrations of cortisol in artificial saliva. b, Sensitivity of bio-FETs in artificial saliva and real human serum.

Supplementary Files

This is a list of supplementary files associated with this preprint. Click to download.

- Supplementaryinformationfinal.docx